Electrical Power and Energy Systems 162 (2024) 110274

Contents lists available at ScienceDirect

International Journal of Electrical Power and Energy Systems

journal homepage: www.elsevier.com/locate/ijepes

Direct modulation in MMC-Based multiterminal hybrid Microgrid: A solution for arm capacitor voltage balancing under unbalanced power distribution

Ahmed G. Abo-Khalil [a,b], Safia Babikir Bashir [b], Mena Maurice Farag [b], Ali A. Adam Ismail [b,c], Abdul-Kadir Hamid [b,c], Nsilulu T Mbungu [b,d,*], Ramesh C. Bansal [b,c,e], A. Elnady [b,c,f], Nirav Patel [g]

[a] Department of Sustainable and Renewable Energy Engineering, University of Sharjah, Sharjah, United Arab Emirates
[b] Research Institute of Sciences and Engineering (RISE), University of Sharjah, Sharjah, United Arab Emirates
[c] Department of Electrical Engineering, University of Sharjah, Sharjah, United Arab Emirates
[d] Department of Electrical Engineering, Tshwane University of Technology, South Africa
[e] Department of Electrical, Electronic and Computer Engineering, University of Pretoria, Pretoria, South Africa
[f] Department of Electrical and Computer Engineering, Royal Military College, Kingston, Canada
[g] ENODA Ltd, Scotland, United Kingdom

ARTICLE INFO

Keywords:
Arm capacitor voltage balancing
Circulating current
carrier phase shift pulse width modulation (CPS-PWM)
Hybrid microgrid
Modular multilevel converter (MMC)

ABSTRACT

The rising interest in hybrid alternating current (AC)/ direct current (DC) microgrids among the global research community can be attributed to the widespread adoption of distributed generation systems (DGs). Therefore, this study applies the modular multilevel converter (MMC) in interconnected microgrids to serve as an interlinking converter involving the AC and DC systems. In this topology, the MMC consists of several submodules (SMs) where a low-voltage direct current (LVDC) microgrid is connected to the output of each SM through a dual active bridge (DAB) converter. As a result of using this topology, more LVDC microgrids can be linked, thus enhancing power transition feasibility. However, during unequal power distribution across LVDC microgrids, the arm capacitor voltage balancing becomes a challenging task and if left unsolved, it will result in unbalanced output voltage at the MMC terminal, thereby affecting the overall system. Therefore, this paper proposes the use of the direct modulation method that is capable of naturally producing fundamental and DC components of the circulating current within the MMC. These circulating current components are responsible for uniformly distributing the energy between the arms of the MMC and balancing the arm capacitor voltage. The effectiveness of the proposed method is further assessed through real-time simulation in the OPAL-RT (OP5700) environment. The findings of this study validate that direct modulation can maintain the optimal performance of a multiterminal hybrid microgrid based on MMC under unbalanced power conditions without applying additional controllers, thus simplifying the system design, and improving the overall efficiency.

1. Introduction

The global electricity demand has significantly increased in recent decades, leading to a greater focus on renewable energy sources as clean and more sustainable option [1–4]. Renewable energy is estimated to make up 90 % of global energy production by 2050 [5–7]. One type of electrical system that has gained popularity for its ability to effectively utilize renewable energy sources is the microgrid [8]. A microgrid is a localized electrical system that can operate individually or is interconnected with the primary power grid. It allows for the integration and efficient consumption of clean energy in various settings, such as remote communities, military bases, and industrial facilities [9].

Microgrids are categorized into three types, based on the type of current flowing on the system: alternating current (AC), direct current

* Corresponding author.
E-mail addresses: aabokhalil@sharjah.ac.ae (A.G. Abo-Khalil), safia.mohamed@sharjah.ac.ae (S. Babikir Bashir), u20105427@sharjah.ac.ae (M. Maurice Farag), aismail@sharjah.ac.ae (A.A. Adam Ismail), akhamid@sharjah.ac.ae (A.-K. Hamid), ntmbungu@ieee.org (N.T. Mbungu), rbansal@sharjah.ac.ae (R.C. Bansal), anady@sharjah.ac.ae (A. Elnady), 2017ree9501@mnit.ac.in (N. Patel).

https://doi.org/10.1016/j.ijepes.2024.110274
Received 18 October 2023; Received in revised form 23 August 2024; Accepted 26 September 2024
Available online 22 October 2024

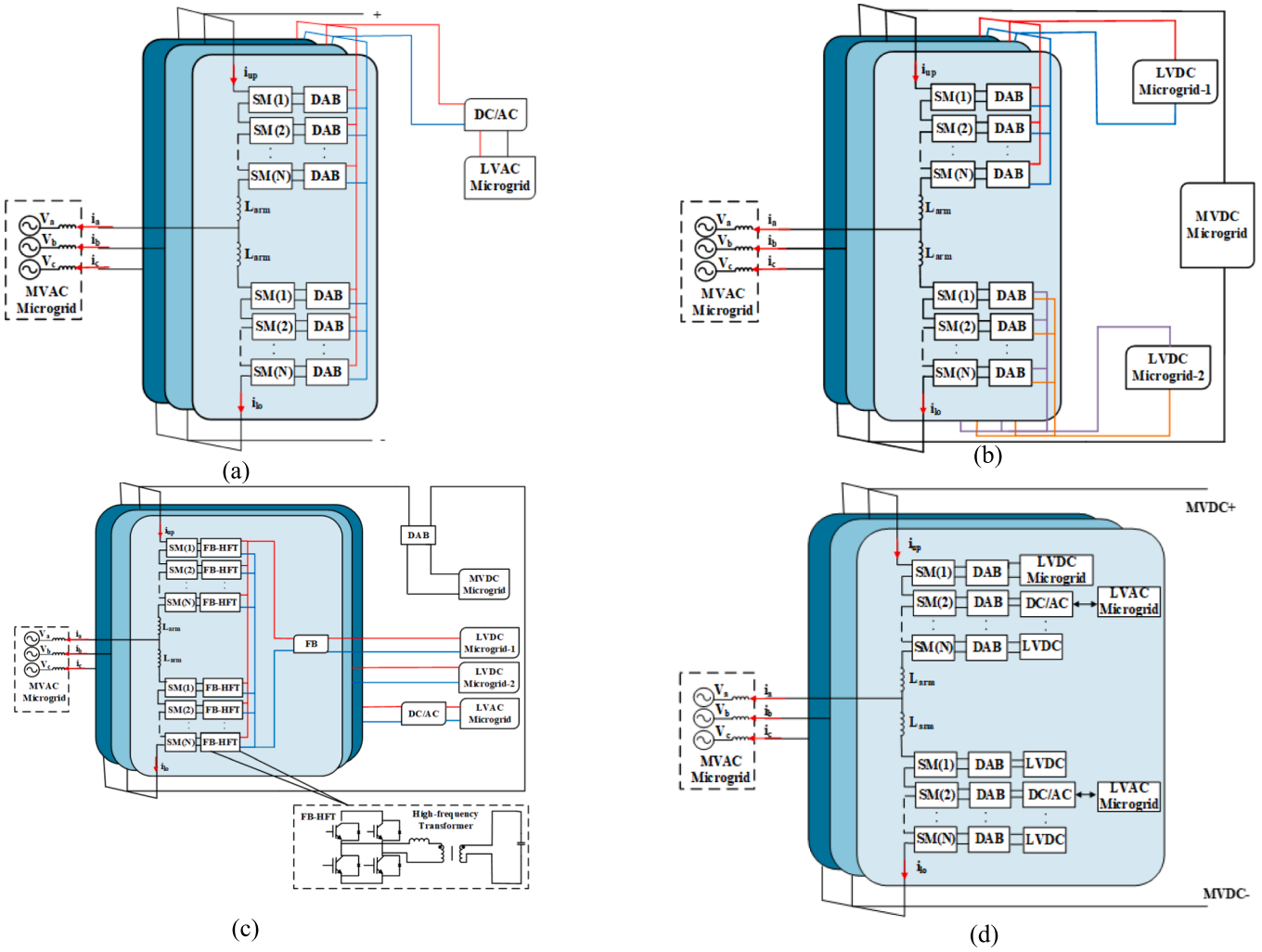

Fig. 1. Proposed MMC-based multiterminal hybrid AC/DC microgrid topologies in literature (a) Topology proposed in [23] (b) Topology proposed in [22] (c) Topology proposed in [24] (d) Topology proposed in [25].

(DC), and AC/DC hybrid microgrids [10,11]. DC microgrids have become attractive in the new generation of power grids due to their techno-economic features for integrating renewable energy and energy storage systems and the increasing demand for DC loads and sources [12,13]. However, the extensive prevalence of AC power systems has made hybrid microgrids emerge as a more pragmatic solution to incorporate both DC and AC microgrid properties [14,15]. Hybrid microgrids have several benefits, including the efficient transmission of power, the ability to convert between DC and AC power, and their existing mutual supports [16].

Conventional hybrid microgrids typically have a single AC and a single DC terminal. These systems have been the focus of extensive research and have proven effective in integrating renewable energy sources and providing backup power during a grid outage [17–21]. Nonetheless, in the last few years, multiterminal hybrid AC/DC microgrids have increasingly gained popularity among scholars. This heightened interest is fueled by their substantial potential for facilitating the comprehensive incorporation of distributed generation systems (DGs) and addressing the expanding necessity for medium and low-voltage (LV) DC power [22].

Multiterminal hybrid AC/DC microgrids naturally necessitate three power conversion stages. Therefore, several research works have suggested the use of a modular multilevel converter (MMC) to serve as an interlinking converter to minimize the number of conversion stages and more effectively satisfy power transmission requirements [22–25]. The MMC is a state-of-the-art multilevel converter configuration, which is exceptionally well-suited to the unique requirements of microgrids [26,27]. The MMC design is inherently modular, providing the ability to easily scale in response to the varying power demands of a microgrid. Additionally, MMCs are distinguished by their high-power density, indicating their proficiency in handling significant power volumes in a compact space [28–30].This feature is especially advantageous in microgrid settings, where space often presents substantial limitations.

Multiterminal hybrid AC/DC microgrids based on MMC have demonstrated their potential for large-scale DG incorporation and catering to the escalating necessity for medium-voltage (MV) and LVDC power [26]. Despite the previous benefits, the issue of controlling uneven power distribution across microgrids remains a considerable challenge that necessitates attention. This imbalance in power distribution can lead to significant repercussions, such as limiting the energy balancing capacity of SMs and causing complications with arm capacitor voltage balancing. Both factors can significantly impact the output voltage of the MMC and the overall system operation.

Several MMC-based multiterminal hybrid AC/DC microgrid topologies and controllers have been developed to enhance the system performance during unbalanced power distributions. In [23], the MMC was used as a power electronic transformer (PET). This configuration combines a dual active bridge (DAB) converter with an MMC half-bridge submodule (SM). Thus, the output terminals of DAB converters are then connected to a LV AC (LVAC) microgrid through a DC/AC power

Table 1
Comparison of MMC-Based Multi-Terminal Hybrid Microgrid Configurations.

Feature	Fig1.a [23]	Fig1.b [22]	Fig1.c [24]	Fig 1.d [25]	This Study
Configuration	Connects one LVAC and one MVAC microgrid	Connects two LVDCs, one MVDC, and one MVAC microgrid	Integrates MVDC, MVAC, two LVDCs, and one LVAC microgrid	Connects multiple LVDC and LVAC microgrids via SM-DABs	Multiple LVDC microgrids connected to the SMs and one MVAC
IGBT Count for N = 4 SM	244	240	170	240 + 4*x (x is the number of LVACs)	240
Advantages	Simple configuration without power balance issues	Enhanced capability under power unbalance conditions	Lower IGBT count enhancing efficiency	Integrates multiple LV microgrids, offering scalability	Integrates multiple LV microgrids, emphasizing scalability
Operational Challenges	Limited power transmission flexibility	Unbalanced power distribution between MMC arms which will affect the arm capacitor voltage balancing	Unbalanced power distribution between MMC phases which will affect the arm capacitor voltage balancing	Severe unbalanced power distribution between MMC arms and phases which will affect arm capacitor voltage balancing	Severe unbalanced power distribution between MMC arms and phases which will affect arm capacitor voltage balancing
Proposed Solution to Operational Challenge	N/A	Inject fundamental and DC circulating current components using additional controllers	Inject fundamental and DC circulating current components using additional controllers	No solution was proposed for arm capacitor voltage balancing during unbalanced power distribution	The use of direct modulation that inherently injects fundamental and DC circulating current components to mitigate power imbalances without using extra controllers

converter. Besides, Fig. 1 (a) illustrates this advanced hybrid microgrid system, which encompasses an LVAC microgrid, an MV AC (MVAC) microgrid, and an MV DC (MVDC) microgrid. Notably, this topology tends to avoid the challenges of unbalanced power distribution since it only involves a single LVAC microgrid. However, its potential is constrained by the limited number of microgrids it incorporates, which results in restricted power transmission flexibility.

To enhance the power transmission flexibility a topology was proposed by [22].This topology connects two LVDCs, one MVDC, and one MVAC microgrids, as demonstrated in Fig. 1(b). However, the nonuniformity of the distributed power between the LVDC microgrids that are linked to the MMC upper and lower arms creates operational challenges for this proposed topology. To address this issue, the control method proposed in [22] involves injecting DC and fundamental frequency circulating current components to mitigate power disparities among the arm. Nonetheless, this approach necessitates additional controllers, which can increase the computation burden.

In order to improve system operation capability and interconnection flexibility during imbalances in power distribution across LVAC and LVDC microgrids, [24] introduces a five-terminal hybrid AC/DC microgrid based on MMC. This setup involves half-bridge SMs linked to Full-Bridge High-Frequency Transformers (FB-HFTs). FB-HFT outputs in phases A and B are integrated with an LVDC microgrid using FB, whereas phase C's output is linked to an LVAC microgrid via a DC/AC converter. Fig. 1 (c) demonstrates the five-terminal system that connects a MVDC microgrid, an MVAC microgrid, two LVDC microgrids, and a LVAC microgrid, increasing the utilization of green energy. However, this topology is influenced by the imbalances in power distribution in the LVDC and LVAC microgrids. To balance the power, controllers must inject DC and AC components of the circulating current, which increases the computational burden.

In [25], a modified MMC under a multiterminal hybrid AC/DC microgrid is presented. This topology is distinct from the previously described topology where each LVDC microgrid is linked to an SM-DAB and each LVAC microgrid is attached to each SM-DAB through a DC/AC converter, as demonstrated in Fig. 1(d). This topology enables the connection of N microgrids, where N represents the number of SMs, thereby enhancing power feasibility. However, uneven power distribution using this topology is severe compared to other reported topologies since power unbalance can occur when there is a difference between the power of microgrids that are connected to the arm and phases of MMC. Despite this limitation, this topology has the potential to be highly promising if the unbalanced power distribution problem can be effectively addressed [26]. Notably, the authors of [25] have not proposed any solutions to address the aforementioned challenges associated with uneven power distribution. Table 1 provides a comparison of the above-mentioned MMC-based multiterminal hybrid AC/DC microgrid configurations.

Therefore, this study proposes the use of the direct modulation method to solve the limited energy balancing capability of the SMs and the arm capacitor voltage balancing issue that arises during unbalanced power distribution. This approach guarantees a balanced output voltage and the proper operation of the overall MMC-based multiterminal hybrid AC/DC microgrid configuration proposed in [25].

The direct modulation method inherently generates fundamental and DC circulating current components within the MMC. These circulating current components will distribute the energy equally among the MMC arms and phases and naturally maintain the arm capacitor voltage balance without needing additional controllers. It is essential to state that the direct modulation scheme is not new and has been used in High Voltage Direct Current (HVDC) application. However, the advantage of using the direct modulation method is not profound in HVDC since the MMC's submodules are not connected to any power source or loads and thus do not suffer from severe arm capacitor voltage balancing issues during unbalanced power distribution. To the author's knowledge, the nature of arm capacitor voltage balancing of the directly modulated MMC in applications other than HVDC was not examined. Thus, the major contribution of this study are:

- Explore the use of direct modulation method, by providing comprehensive mathematical equations that explain its capability in maintaining arm capacitors voltage balance under unbalanced power distribution. Therefore, this study is the first to consider applying direct modulation strategy to address the issue of severe unbalanced power distribution between MMC-based microgrid arms and phases.
- Eliminate the need for additional controllers to induce necessary circulating current components for arm voltage balancing.

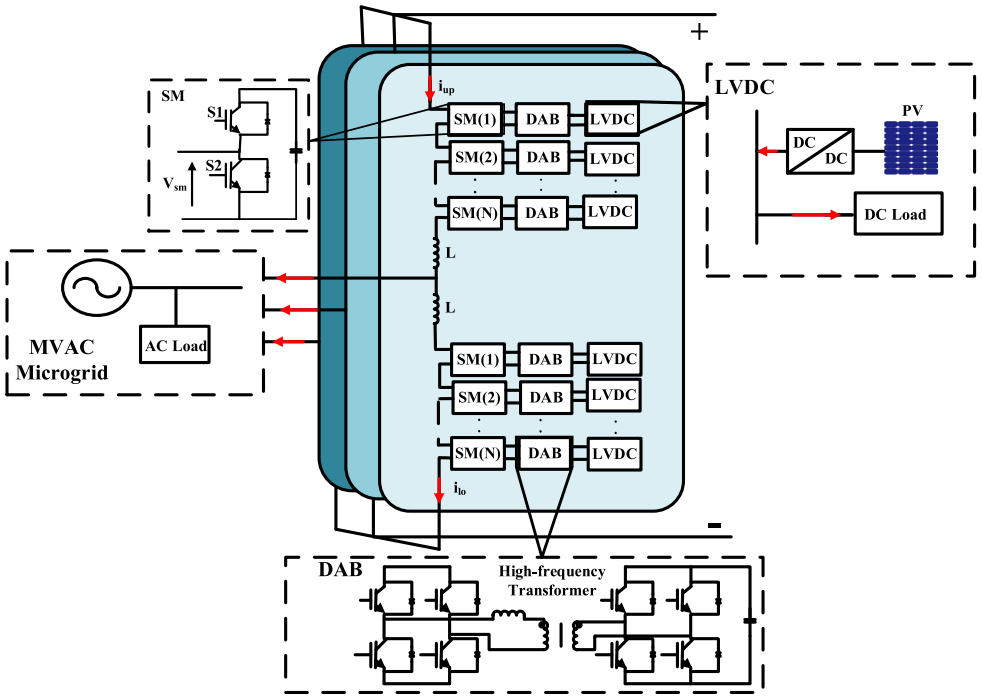

Fig. 2. Multiterminal hybrid AC/DC microgrid based on MMC.

Therefore, the direct modulation approach simplifies the system design and improves efficiency. Besides, the proposed direct modulation technique ensures consistent output voltage at the MMC's output terminal, enhancing the overall performance of the microgrid system.

- Comparatively assessing the effectiveness of the direct modulation technique with respect to the indirect modulation method, highlighting the advantages and limitations of both applied techniques, and validate the effectiveness of the direct method through real-time simulation via OPAL-RT (OP5700), under unbalanced power distribution scenarios.
- Fill the knowledge gap in the importance of using the direct modulation method beyond HVDC applications, providing prospects in optimizing its deployment for complex microgrid structures.

The basic structure and operation of the MMC-based hybrid microgrid are explained in detail in Section 2. Section 3 describes the direct modulation technique and the principle behind its ability to balance arm capacitor voltage. A description of the control scheme of the MMC-based hybrid microgrid is provided in Section 4. Section 5 presents the real-time simulation outcomes of the suggested approach under different scenarios. Finally, the conclusions and observations drawn from this study are presented in Section 6.

2. MMC based multiterminal hybrid microgrid

2.1. System configuration

In this paper, the MMC serves as an interlinking converter, merging N LVDC microgrids with an MVAC Microgrid. Each LVDC microgrid is interconnected to the MMC's SM through a DAB, as illustrated in Fig. 2. The DAB converter regulates the voltage levels at LVDC terminals and facilitates the transmission of DC power. As demonstrated in Fig. 2, the DAB converter consists of two full-bridge converters, a high-frequency transformer, and an output capacitor, all of which contribute to its ability to offer a broad range of voltage adjustment options. In this paper, the LVDC microgrid is depicted by a PV system and DC load, while the AC system is represented by an AC source and AC load as shown in Fig. 2.

The MMC is capable of generating MV sinusoidal waveforms using LV components without the need to connect these components in series [31–33]. The MMC circuit configuration in Fig. 2 involves arranging the SMs in series [31–33]. Each phase of the m-level MMC is called a leg, and every leg is divided into upper and lower arms, with each arm containing N SMs, where N resembles the number of SMs. Each SM consists of a half-bridge (HB) converter with a DC capacitor. The HB switches, S1 and S2, control the current flowing through the SM, and the DC capacitor acts as a voltage source. When S1 is on and S2 is off, the SM is connected to the circuit, and the terminal voltage is equal to the capacitor voltage. The polarity of the arm current determines the charging or discharging of the capacitor; if the current is positive, the capacitor is charged through the upper diode. If the current is negative, the capacitor is discharged. When S2 is on and S1 is off, the SM is bypassed, and the capacitor voltage remains constant. The switches must be used complementarily to prevent the capacitor from being shorted. By controlling the number of inserted and bypassed SMs, the MMC produces a staircase output voltage at its AC terminals. Besides, the arm inductors (L) restrict the circulating current within the MMC.

2.2. Problem description

In general, a multiterminal hybrid AC/DC microgrid-based MMC offers significant advantages regarding power feasibility due to the high number of LVDC microgrids that can be interconnected. However, the power imbalance resulting from variations in the power distribution between the LVDC microgrids poses a significant challenge to the proper functioning of the system. In this topology, two types of power imbalances can occur: inter-phase and inter-arm imbalances. The inter-phase imbalance arises from power variations in the LVDC microgrids among the different phases. In contrast, the inter-arm imbalance occurs when the power of the LVDC microgrids in the upper arm differs from that of the LVDC microgrids in the lower arm.

Generally, the power imbalance will lead to unbalanced arm capacitor voltages, which will result in an unbalanced output voltage at the MMC and, by extension, the overall performance of the multiterminal hybrid microgrid system. Addressing the power imbalance issue is

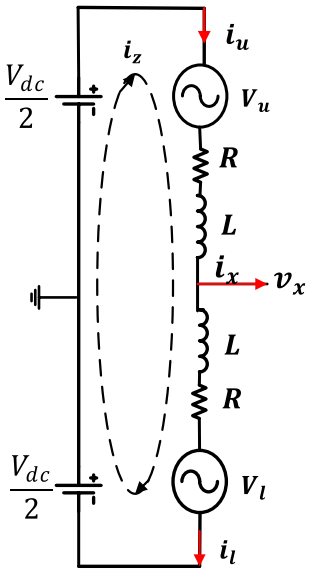

Fig. 3. Single phase topology of MMC.

crucial for ensuring the proper operation of the MMC within the framework of the multiterminal hybrid microgrid.

2.3. Modelling

In this subsection, the mathematical representation of the MMC is delved in to assist in the design process of the control system and better comprehend the dynamics of direct and indirect modulation. To simplify the analysis, the individual SMs of each arm in the MMC are illustrated by a single voltage source expressed as v_u and v_l, as presented in Fig. 3. To establish a mathematical model, the single-phase MMC is utilized.

In principle, Kirchhoff's circuit laws can be employed to formulate the following expressions:

$$\frac{v_{dc}}{2} - v_x = v_u + Ri_u + L\frac{di_u}{dt} \tag{1}$$

$$\frac{v_{dc}}{2} + v_x = v_l + Ri_l + L\frac{di_l}{dt} \tag{2}$$

$$i_x = i_u - i_l \tag{3}$$

where the lower and upper arms currents are represented by i_l and i_u, respectively. The arm's overall resistance and inductance are denoted by R and L, respectively. While i_x and v_x represent the output current and voltage, respectively.

The currents in the arm comprise a circulating current and an alternating output current [34], as demonstrated in (4) and (5):

$$i_u = \frac{i_x}{2} + i_z \tag{4}$$

$$i_l = -\frac{i_x}{2} + i_z \tag{5}$$

where the circulating current is denoted by i_z and can be expressed as

$$i_z = \frac{i_l + i_u}{2} \tag{6}$$

Furthermore, (7) can be obtained by subtracting (1) from (2) and substituting $i_u - i_l$ by i_x

$$\frac{v_l - v_u}{2} = v_x + \frac{R}{2}i_x + \frac{L}{2}\frac{di_x}{dt} \tag{7}$$

The summation of (2) and (1) and employing (6) yields the following expression.

$$L\frac{di_z}{dt} + Ri_z = \frac{v_{dc}}{2} - \frac{v_l + v_u}{2} \tag{8}$$

To simplify the analysis, the term $\frac{v_l - v_u}{2}$ in (7) can be represented as e_x, which represents the internal electromotive force (emf) of the MMC that drives the output current, while the term $\frac{v_{dc}}{2} - \frac{v_l + v_u}{2}$ in (8) is represented with v_z.

The voltage of the upper and lower arms can be formulated in the following forms.

$$v_u = \frac{v_{dc}}{2} - e_x - v_z \tag{9}$$

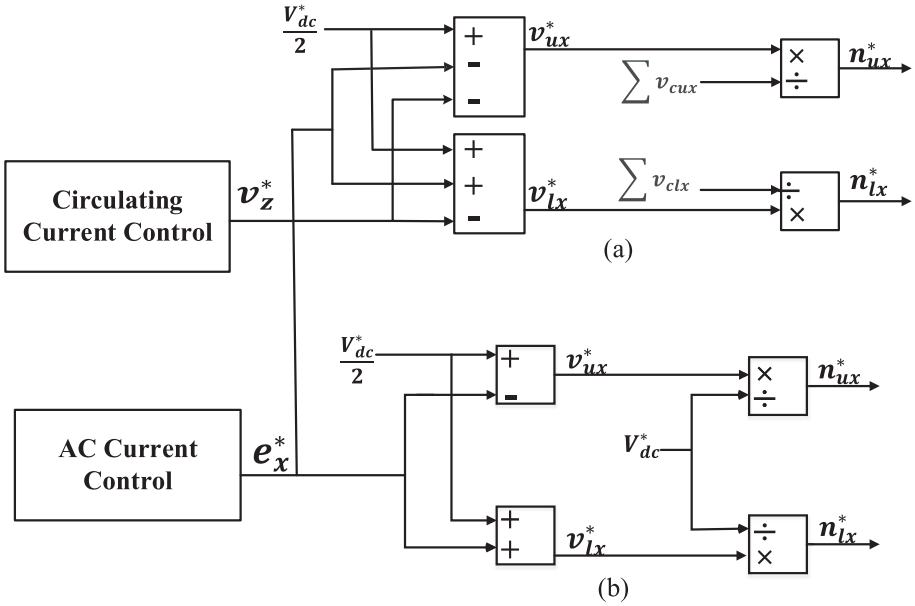

Fig. 4. (a) indirect modulation method (b) direct modulation method.

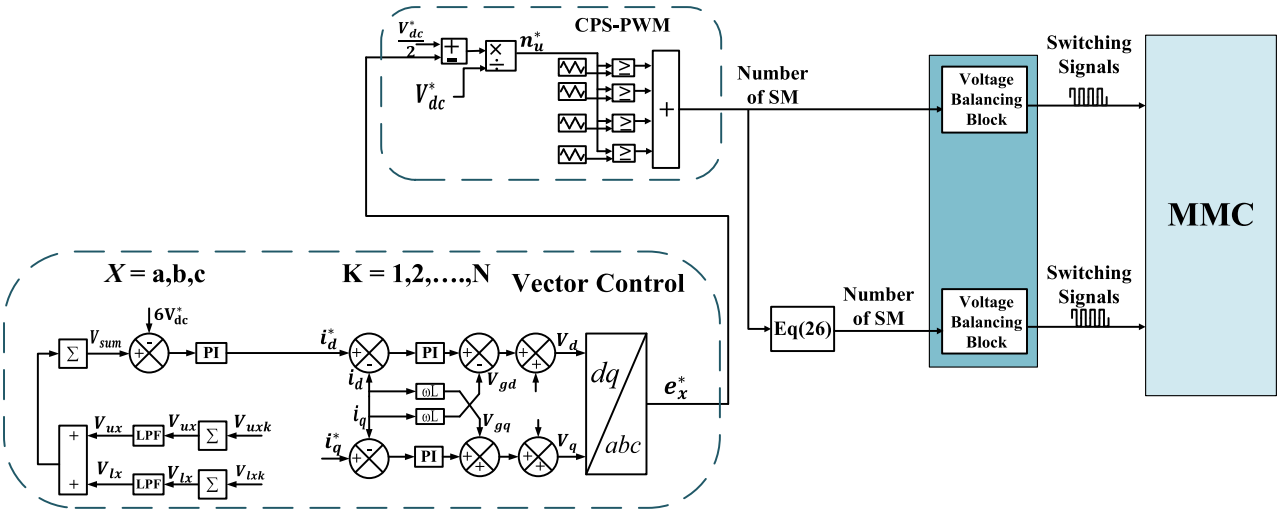

Fig. 5. MMC Control System.

$$v_l = \frac{v_{dc}}{2} + e_x - v_z$$

3. Direct modulation

In this study, the direct modulation method is proposed to ensure the proper operation of the MMC in the presence of unequal power distribution in LVDC microgrids connected to the SMs of the MMC. The first subsection provides an overview of the direct modulation method and compares it with the indirect modulation approach. The second subsection details how the direct modulation approach can effectively balance arm capacitor voltage in the presence of unbalanced power among LVDC microgrids.

3.1. Comparison between direct and indirect modulation techniques

Modulation techniques for MMCs can be divided into direct and indirect. The indirect modulation method determines the normalized arm's reference voltage ($v^*_{ux} and v^*_{lx}$) based on the voltage levels of the submodule capacitors in each arm ($\sum v_{cux} and \sum v_{clx}$), as illustrated in Fig. 4(a) [35,36]. This method produces a 2 N + 1 voltage level and inherently prevents the twice-line frequency component in the circulating current but requires a closed-loop controller to stabilize the arm capacitor voltage. On the contrary, in the direct modulation method, the arm reference voltages (v^*_{ux} and v^*_{lx}) are normalized based on the rated DC bus voltage (v^*_{dc}) as demonstrated in Fig. 4(b). Thus, in this method, the number of inserted cells in the upper and lower arms remains constant (N) [37].

This method has the drawback of causing a twice-line frequency component in the circulating current due to the instability of the SM capacitor voltage. This issue can be mitigated by increasing the arm inductor (L). However, the direct modulation method has a unique property of naturally balancing the arm capacitor voltage without the need for using a closed loop controller, which can be of great use in an MMC-based multi-terminal hybrid microgrid. Fig. 4 demonstrates the difference between direct and indirect modulation method in obtaining the insertion ratios of MMC arms ($n^*_{ux} and n^*_{lx}$) where e^*_x represents the inner emf reference voltage obtained from the vector control that drives the AC grid current, v^*_{dc} is rated DC bus voltage, v^*_z is the voltage that drives or controls the circulating current.

3.2. Role of direct modulation in MMC-Based multiterminal hybrid microgrid

The uneven power distribution in the LVDC microgrids in Fig. 2 will result in variable power consumption across the MMC arms and phases. This, in turn, will cause the sum and the difference of the upper and lower arm capacitor voltage of each phase to drift from its equilibrium. The direct modulation method will inherently induce a DC component of the circulating current when the sum of the upper and lower arm capacitor voltage of each phase drifts from equilibrium and a fundamental current component when the difference between the upper and lower arm capacitor voltage drifts from equilibrium. These induced circulating current components will transfer energy among the arms. Therefore, the SM capacitor voltages within the arm are maintained at their designated values, ensuring that a balanced output voltage is produced.

To gain an understanding of why this happens when direct modulation is used, it's essential to use the MMC mathematical model.

The reference voltages for the upper and lower arms of the MMC, which are derived from (9) and by neglecting the term v_z is given as flows.

$$v^*_{ux} = \frac{V^*_{dc}}{2} - e^*_x \tag{10}$$

$$v^*_{lx} = \frac{V^*_{dc}}{2} + e^*_x \tag{11}$$

where e^*_x represents the inner emf reference voltage obtained from the vector control that drives the AC grid current.

The insertion ratio of the arms in the direct modulation method, according to its definition and as illustrated in Fig. 4 is as follows:

$$n^*_{ux} = \frac{v^*_{ux}}{V^*_{dc}} = \frac{\frac{V^*_{dc}}{2} - e^*_x}{V^*_{dc}} = \frac{1}{2} - \frac{e^*_x}{V^*_{dc}} \tag{12}$$

$$n^*_{lx} = \frac{v^*_{lx}}{V^*_{dc}} = \frac{\frac{V^*_{dc}}{2} + e^*_x}{V^*_{dc}} = \frac{1}{2} + \frac{e^*_x}{V^*_{dc}} \tag{13}$$

Thus, the actual voltage of the arms can be determined by

$$v_{ux} = n^*_{ux} \sum v_{cux} = \left(\frac{1}{2} - \frac{e^*_x}{V^*_{dc}}\right) \sum v_{cux} \tag{14}$$

$$v_{lx} = n^*_{lx} \sum v_{clx} = \left(\frac{1}{2} + \frac{e^*_x}{V^*_{dc}}\right) \sum v_{clx} \tag{15}$$

where $\sum v_{cux}$ and $\sum v_{clx}$ represent the total capacitor voltages of the SMs in the upper and lower arms, respectively. Since the time derivative of energy is power, the upper and lower arm power can be computed by multiplying the arm voltage by the arm current.

$$\frac{dE_{ux}}{dt} = P_{ux} = v_{ux} i_{ux} = (n^*_{ux} \sum v_{cux}) i_{ux} \tag{16}$$

$$\frac{dE_{lx}}{dt} = P_{lx} = v_{lx} i_{lx} = (n^*_{lx} \sum v_{clx}) i_{lx}$$

The change in the arm capacitor energy can further be represented in detail as:

$$\frac{dE_{ux}}{dt} = C \sum_{i=1}^{N} v_{cux[i]} \frac{dv_{cux[i]}}{dt} \cong \frac{C}{2N} \frac{d\left(\sum v_{cux}\right)^2}{dt} = \frac{C}{N} \sum v_{cux} \frac{d \sum v_{cux}}{dt} \tag{17}$$

$$\frac{dE_{lx}}{dt} = C \sum_{i=1}^{N} v_{clx[i]} \frac{dv_{clx[i]}}{dt} \cong \frac{C}{2N} \frac{d\left(\sum v_{clx}\right)^2}{dt} = \frac{C}{N} \sum v_{clx} \frac{d \sum v_{clx}}{dt}$$

Then by substituting (17), (14), and (15) into (16) and by replacing (i_{ux} and i_{lx}) by their equivalent in (4 and 5), the dynamics of the energy and arm capacitor voltage are obtained.

$$\frac{dE_{ux}}{dt} = \frac{C}{N} \frac{d \sum v_{cux}}{dt} = n^*_{ux} i_{ux} = \left(\frac{1}{2} - \frac{e^*_x}{V^*_{dc}}\right)\left(\frac{i_x}{2} + i_z\right) \tag{18}$$

$$\frac{dE_{lx}}{dt} = \frac{C}{N} \frac{d \sum v_{clx}}{dt} = n^*_{lx} i_{lx} = \left(\frac{1}{2} + \frac{e^*_x}{V^*_{dc}}\right)\left(\frac{-i_x}{2} + i_z\right)$$

The sum and the difference energy of (18) in each phase are given below.

$$\frac{d(E_{ux} + E_{lx})}{dt} = \frac{d(\sum E_x)}{dt} = \frac{1}{V^*_{dc}} \left(V^*_{dc}\, i_z - e^*_x i_x\right) \tag{19}$$

$$\frac{d(E_{ux} - E_{lx})}{dt} = \frac{d(\Delta \mathrm{E_x})}{dt} = \left(\frac{i_x}{2} - \frac{2 e^*_x i_z}{V^*_{dc}}\right)$$

From (19), it can be concluded that the total sum of arm capacitor energy, $\sum E_x$, of each phase is affected by the DC component of the circulating current. On the contrary, the DC component of the circulating current does not affect the difference arm capacitor energy, ΔE_x, since e^*_x contains no DC component. Thus, according to (19), the difference in arm capacitor energy, ΔE_x, is affected by the fundamental frequency component of the circulating current.

The direct modulation technique can produce a fundamental frequency and DC component in the circulating currents inherently. This can be explained as follows:

The total voltage of the SMs capacitors within each arm is:

$$\sum v_{cux} = V^*_{dc} \tag{20}$$

$$\sum v_{clx} = V^*_{dc}$$

Thus, the sum and the difference of the SMs capacitors in each phase can be described as:

$$\sum v_{cx} = \sum v_{cux} + \sum v_{clx} = 2V^*_{dc} \tag{21}$$

$$\Delta v_{cx} = \sum v_{cux} - \sum v_{clx} = 0$$

Rewriting (8) that covers the circulating current dynamics as:

$$L \frac{di_z}{dt} + R i_z = \frac{1}{2}\left(V_{dc} - (v_{ux} + v_{lx})\right) \tag{22}$$

and by adding v_{ux} and v_{lx} in (14) and (15), the following is obtained:

$$v_{ux} + v_{lx} = \frac{1}{2}\left(\sum v_{cux} + \sum v_{clx}\right) + \frac{e_x}{V^*_{dc}} \left(\sum v_{clx} - \sum v_{cux}\right. \tag{23}$$

By substituting (23) in (22) it can be expressed as:

$$L \frac{di_z}{dt} + R i_z = \frac{1}{2}\left(V_{dc} - \left(\frac{1}{2}\left(\sum v_{cux} + \sum v_{clx}\right) + \frac{e_x}{V^*_{dc}} \left(\sum v_{clx} - \sum v_{cux}\right)\right)\right) \tag{24}$$

According to (21) $\sum v_{cux} + \sum v_{clx}$ can be replaced by $\sum v_{cx}$ and $\left(v_{cxl}^{\sum} - v_{cxu}^{\sum}\right)$ can be replaced by $-\Delta v_{cx}$. Thus, (24) becomes as follows:

$$L \frac{di_z}{dt} + R i_z = \frac{1}{2}\left(V_{dc} - \frac{\sum v c_x}{2} + \frac{e_x}{V^*_{dc}} (\Delta v c_x)\right) \tag{25}$$

From (25), it can be observed that when $\sum v_{cx}$ drift from $2V^*_{dc}$ due to the changes in the power distribution between LVDC, will trigger a DC component in the circulating current. Alternatively, if $\Delta v c_x$ diverges from zero, it inherently prompts a fundamental frequency component within the circulating current. The naturally induced circulating current components due to the use of direct modulation will transfer the energy among the arms. As a result, the arm capacitor voltages will remain at their rated voltages, resulting in a proper output voltage.

On the other hand, the insertion ratio of the arms in the indirect modulation method according to its definition and Fig. 4 is as follows:

$$n^*_{ux} = \frac{v^*_{ux}}{\sum v_{cux}} = \frac{\frac{V^*_{dc}}{2} - e^*_x}{\sum v_{cux}} \tag{26}$$

$$n^*_{lx} = \frac{v^*_{lx}}{\sum v_{clx}} = \frac{\frac{V^*_{dc}}{2} + e^*_x}{\sum v_{clx}}$$

Thus, the actual voltage of the arms can be determined by

$$v_{ux} = n^*_{ux} \sum v_{cux} = \left(\frac{\frac{V^*_{dc}}{2} - e^*_x}{\sum v_{cux}}\right) \sum v_{cux} = \frac{V^*_{dc}}{2} - e^*_x \tag{27}$$

$$v_{lx} = n^*_{lx} \sum v_{clx} = \left(\frac{\frac{V^*_{dc}}{2} + e^*_x}{\sum v_{clx}}\right) \sum v_{clx} = \frac{V^*_{dc}}{2} + e^*_x \tag{28}$$

by adding v_{ux} and v_{lx} in (27) and (28), the following is obtained:

$$v_{ux} + v_{lx} = V^*_{dc} \tag{29}$$

By substituting (29) in (8):

$$L \frac{di_z}{dt} + R i_z = \frac{1}{2}\left(V_{dc} - V^*_{dc}\right) \tag{30}$$

From (30), it can be concluded that the indirect modulation method is not capable of inherently inducing a DC and the fundamental component is the circulating current. Therefore, a circulating current controller is introduced to inject these components by using the term v_z, as shown in Fig. 4.a as a result (30) becomes:

$$L \frac{di_z}{dt} + R i_z = \frac{v_{dc}}{2} - v_z \tag{31}$$

4. Control method

The control system of the MMC-based multiterminal microgrid consists of one carrier phase shift pulse width modulation (CPS-PWM), two balancing blocks, and vector control, as shown in Fig. 5, which will be explained in this section.

4.1. Vector control

The vector control approach is employed to regulate the AC current output of the MMC in the multiterminal microgrid. This technique

regulates the voltage converter to comply with a current reference injected into the AC system. This control approach necessitates converting currents and voltages from the ABC reference frame into a DQ synchronous reference frame. A significant advantage of vector control is the appearance of AC voltage and current vectors as steady constants post-DQ transformation, allowing simple PI controllers to mitigate static errors. This control scheme is implemented as a cascaded structure consisting of two successive control loops, where the outer loop supplies the set points for the inner current control loops. As depicted in Fig. 5, the active current reference, denoted as i_d^*, is derived from a PI controller which takes into account the voltage discrepancy between the total voltage across all submodule capacitors and its set point, represented by $6V_{dc}^*$. If the total capacitor voltage falls below $6V_{dc}^*$, an active current is absorbed by the MMC. Conversely, when the cumulative capacitor voltage surpasses $6V_{dc}^*$, the MMC introduces active current into the system. The reactive current reference is denoted as i_q^*, and determined by the MVAC grid's reactive power needs for compensatory purposes. This is expressed as $i_q^* = 2{*}QMVAC/3Vg$, where $QMVAC$ signifies the reactive power dispatched from the MVAC grid, and Vg represents the amplitude of the MVAC grid voltage. To find the requisite phase angle for shifting voltages and currents between the ABC and DQ reference frames and vice versa, a Phase Locked Loop (PLL) is employed. The inner control loop then produces the needed q-axis (v_q) and d-axis (v_d) voltage elements. Once these voltages are produced, they're transposed to the ABC reference frame (represented as v_a, v_b , v_c) and forwarded to the CSP-PWM block.

In addition to controlling the MMC, DAB converters that are used to connect the LVDC microgrid to the SM need to be controlled. More information about the control of DAB converters is found in [38].

4.2. CPS-PWM

Multilevel converters work on the fundamental idea of creating a sinusoid voltage out of discrete voltage levels. Pulse-width-modulation (PWM) strategies can be used to achieve this. Numerous PWM strategies tailored to multilevel converters have been established [24,25,31]. The carrier phase shift pulse width modulation (CPS-PWM) is among the most popular PWM techniques used for MMC. In CPS-PWM, the modulation reference of each phase obtained from the vector control is compared with multiple carrier waveforms to generate the number of SM that need to be turned on in the upper arms of the MMC, as demonstrated in Fig. 5. It is worth noting that in this paper, only one CPS-PWM is used. The number of SMs in the lower arm is determined by the complement of the upper arm, as per (32). This effectively removes the necessity for a separate CPS-PWM for the lower arm. The rationale behind discarding the second CPS-PWM is based on the observation that in direct modulation, the total number of SMs incorporated in each phase equals N, where N denotes the number of SMs per arm. The use of only one CPS-PWM will reduce the system computation burden. In addition, it will facilitate the inherent generation of the DC and fundamental component in the circulating current during imbalanced power distribution in the Microgrids.

$$N_{lo} = N - N_{up} \tag{32}$$

4.3. Balancing method

In the effective operation of a Modular Multilevel Converter (MMC), maintaining a balance in the capacitor voltages of each submodule (SM) is crucial. This study utilizes the 'sorting method' to establish this balance. This procedure entails organizing the capacitor voltage of every SM in an ascending or descending sequence. Subsequently, the SM possessing the lowest voltage is selected and inserted during the arm current's positive flow, thereby charging it. Conversely, when the arm current flows in the negative direction, the SM with the highest voltage is inserted, facilitating the capacitor's discharge. An in-depth exploration of the steps necessary to apply this voltage balancing method can be found in [39].

5. Results and Discussion

The real-time simulation is conducted in this section to validate the effectiveness of the direct technique in preserving the stable operation of the MMC-based microgrid during unbalanced power distribution. The model of the MMC-based multiterminal microgrid was developed in Simulink/MATLAB and then tested using the OP5700 platform from OPAL-RT Technologies, as illustrated in Fig. 6. The developed three-phase five-level MMC uses four SMs, four DABs, and four LVDC microgrids in each arm, resulting in 24 SMs, 24 DABs, and 24 LVDC microgrids in total. In addition, one MVAC microgrid is connected to the AC output terminal. Table 2 provides the parameters of the MMC-based hybrid microgrid that are utilized in the real-time simulation. These parameters are selected based on relevant international standards to ensure compatibility and safety in microgrid applications. The MVAC microgrid voltage of 3 kV was chosen in accordance with IEC Standard 60038. For the LVDC microgrid that was selected, following the European Union Low Voltage Directive (LVD) 2006/95/EC. Additionally, the design of

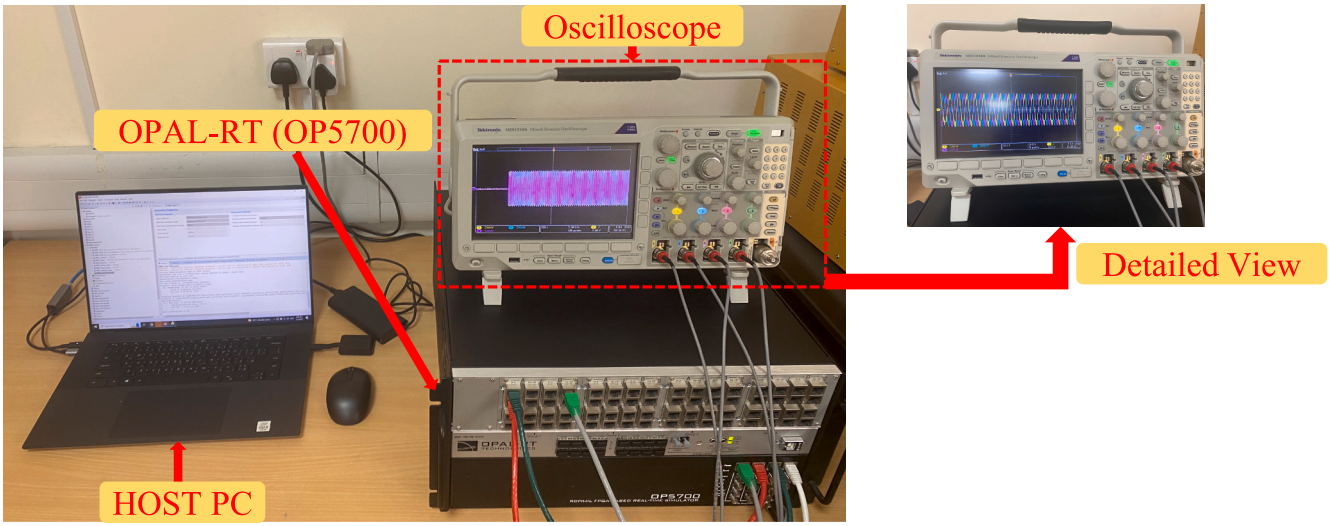

Fig. 6. Real-time simulation setup.

Table 2
System Parameters.

MMC − parameters	
SM capacitance	C = 2600H
Arm inductance	L = 1.59mH
SM average voltage	V_{sm_avg} = 1500V
Switching frequency	f_{sw} = 5KHz
Number of levels	N = 5
MVAC Microgrid	
Voltage	V_{MVAC} = 3kV
Rated power	P_{MVAC} = 2.4Mw
LVDC Microgrid	
Rated DC voltage	V_{LVDC} = 400
Rated power	P_{LVDC} = 1 00 kW
DAB converter	
Switching frequency (f_{sw})	4kHz
DC capacitance	1mF
Input voltage	1500 V
Leakage inductance	0.5mH

the MMC was based on these specified MVAC and LVDC voltage levels to ensure optimal performance and integration within the microgrid system.

It is worth mentioning that the real-time suite caters to signals within a specified voltage range at the Analog to Digital Converter (ADC) terminals, thus mandating the step-down of the MMC-based hybrid microgrid parameters for proper observation of the results via a 4-channel oscilloscope. The case studies that are used to validate the effectiveness of the direct and indirect modulation are given in Table 3.

5.1. Case1

Initially, all the LVDC microgrid's power is set to 100kW. At t = 0.9 s, the power level of each LVDC Microgrid of phase-a is changed from 100kW to 50kW. In this notion, the total power of the microgrids of phase-a (P_A) is decreased from 800kW (8*100kW) to 400kW (8*50kW) as depicted in Fig. 7(a). Meanwhile, the power levels of the microgrids in the other phases remain unchanged, creating an imbalance in power distribution between the phases. The imbalance in the power distribution between LVDC microgrids causes the sum voltages, $\sum v_{cx}$, to drift from $2V_{dc}$, as presented in Fig. 7(b). According to (25), the drift of the sum voltage when the direct modulation is used will inherently induce a DC component in the circulating current, as demonstrated in Fig. 7(c). This study makes a key contribution by demonstrating the direct modulation method's capability to induce a DC component in the circulating current in response to this deviation. This DC component effectively balances the arm capacitor voltages at their rated value of 1500 V, despite power imbalance, as shown in Fig. 7(d). The successful balancing of the arm capacitor voltages resulted in a balanced output voltage, as illustrated in Fig. 7(e).

A key measure of the effectiveness of the direct modulation strategy is the Total Harmonic Distortion (THD). A slight variation was observed in the THD of phase-a voltage before and after t = 0.9 s, marginally dipping from 17.56 % to 17.40 %. This marginal change supports the argument that direct modulation managed to maintain consistently high voltage quality despite unbalanced power distribution in LVDC microgrids.

On the other hand, when the indirect modulation method is used, no DC component is induced in the circulating current, as shown in Fig. 8 (a). Therefore, the unequal power distribution of LVDC microgrids results in the arm capacitor voltage of phase a drifting from its rated value (1500 v), as illustrated in Fig. 8(b). This substantial and non-steady drift in arm capacitor voltage has affected the output voltage of phase-a and resulted in an unbalanced output voltage, as presented in Fig. 8(c). With the indirect modulation method, the THD of phase-a voltage has increased significantly from 9.51 % before t = 0.9 s to 22.31 % after the event. This vivid increase emphasizes the challenges inherent in the indirect modulation approach under conditions of unequal power distribution. In addition, the results also suggest a potential necessity for controllers to induce a DC component in the circulating currents, thereby achieving the required balancing of arm capacitor voltages.

It's worth noting that before the power shift at t = 0.9 s, the THD in the indirect modulation method was lower than in the direct modulation method. This can be attributed to the inherent capacity of the indirect modulation method to produce an output voltage level of 2 N + 1, compared to the direct modulation method, which can only achieve N + 1 levels.

5.2. Case2

In this case, each LVDC microgrid has a power capacity set at 100kW. However, at t = 0.9 s, the power of each LVDC microgrid in the upper arm of phase-a is scaled down to 50 kW. This power reduction leads to a corresponding decrease in the generated power of phase-a from 800kW (8*100kW) to 600kW (4*50kW +4*100kW) (P_A), as depicted in Fig. 9(a), with the power levels of the remaining phases staying constant. The unbalanced power between the arms (upper and lower) initiates a substantial deviation in Δv_{cx} from its equilibrium state ($\Delta v_{cx} \cong 0$), as shown in Fig. 9(b).

Thus, when direct modulation is used, it inherently induces an AC component in the circulating current according to (25).

Table 3
Description of case studies implemented using direct and indirect modulation.

Case	Time	Phase a		Phase b		Phase c	
		Upper arm total power	Lower arm total power	Upper arm total power	Lower arm total power	Upper arm total power	Lower arm total power
1	After 0.9 s	200kW	200kW	400kW	400kW	400kW	400kW
2	After 0.9 s	200kW	400kW	400kW	400kW	400kW	400kW
3	After 0.5 s	200kW	200kW	400kW	400kW	400kW	400kW
	After 1 s	200kW	200kW	200kW	400kW	400kW	400kW

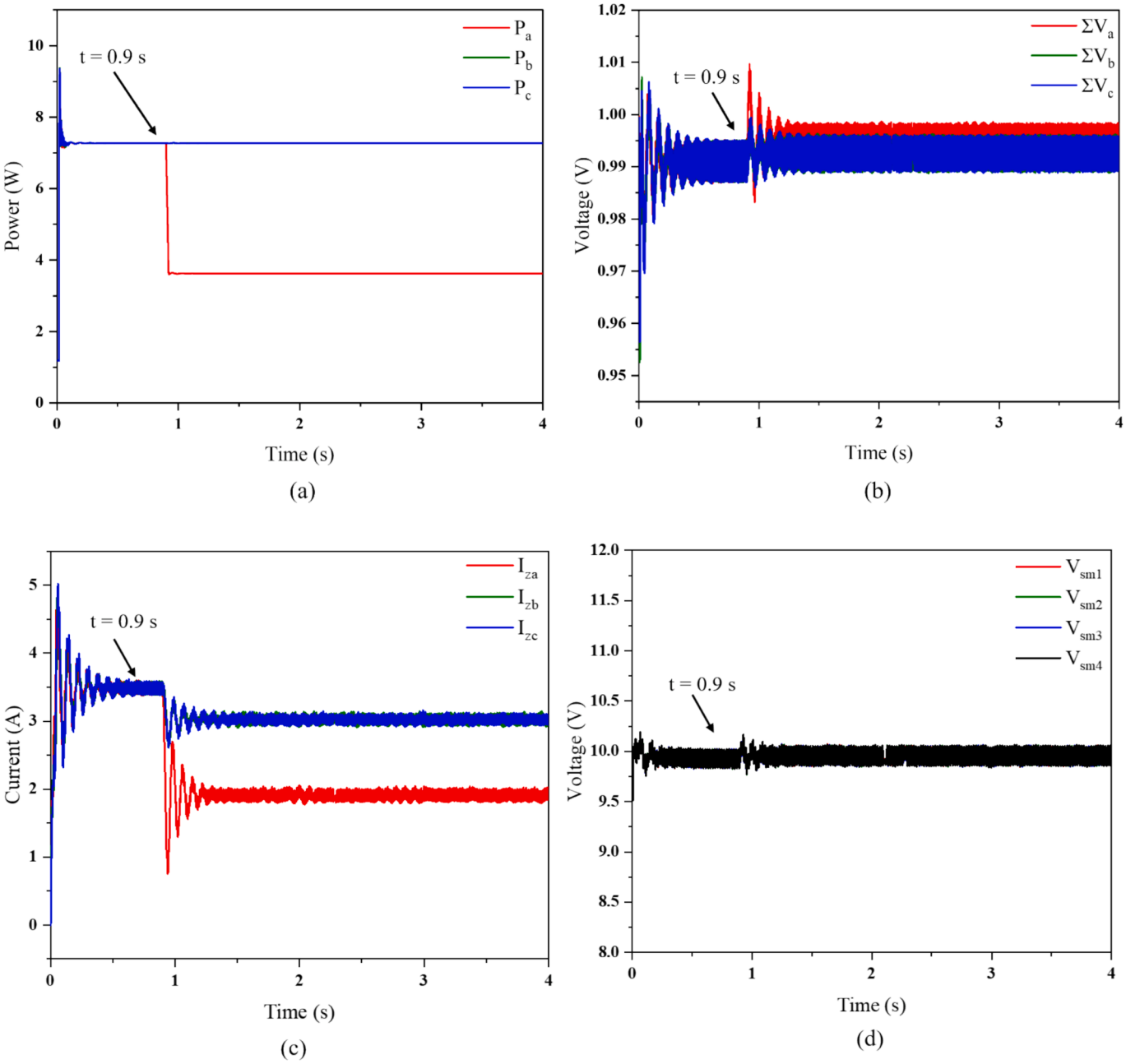

Fig. 7. Case 1: Direct modulation (a) total power of microgrids, (b) $\sum V_x$, (c) Circulating current, (d) SMs capacitor voltages, (e) MMC output voltage.

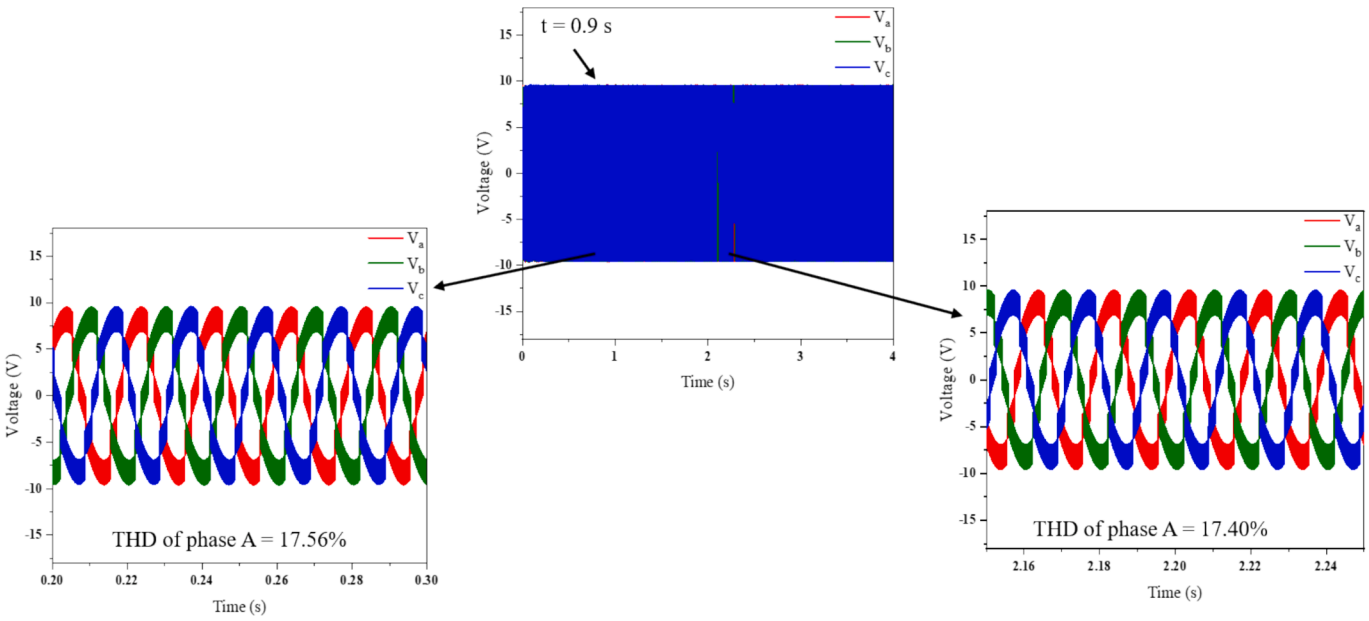

(e)

Fig. 7. (*continued*).

The imbalance between the arms power does not merely impact the arm; it also disrupts the power balance among the three phases. Consequently, a DC circulating current emerges along with the AC circulating current, as revealed in Fig. 9.c. Fig. 9(d) shows that the induced circulating current components could effectively balance the arm capacitor voltages despite the uneven power distribution between the LVDC microgrids, which led to a balanced output voltage, as illustrated in Fig. 9(e). Only a slight variation was observed in the THD of phase-a voltage before and after t = 0.9 s, marginally increasing from 17.59 % to 17.67 %.

In contrast, when using the indirect modulation method, it can be observed that no components are induced in the circulating current, as presented in Fig. 10(a). This resulted in unbalanced arm capacitor voltages, as illustrated in Fig. 10(b). which affects the MMC output voltage balance, as shown in Fig. 10(c). Thus, in this case, the THD of phase a has increased from 8.99 % to 18.50 %.

5.3. Case3

To further examine the capability of the direct modulation in balancing the arm voltage, a third case is introduced where both the arm and phase power imbalance occurs. Initially, each LVDC microgrid has a power capacity at $100kW$ and at t = 0.5 s, the power of each LVDC microgrids in phase-a is reduced to $50kW$. Then at t = 1 s the power of each LVDC microgrid that is connected to the upper arm of phase-b is reduced to $50kW$. Fig. 11(a) illustrates the change in power of each phase. The unbalanced power between the phases and arms has led to a substantial deviation in $\sum v_{cx}$ from $2V_{dc}$, and Δv_{cx} from 0 as depicted in Fig. 11(b) and Fig. 11(c). According to (25), the drift of $\sum v_{cx}$ from $2V_{dc}^{*}$ will induce a DC component in the circulating current when the direct modulation is used, as it can be observed in Fig. 11(d). On the other hand, it can be concluded from (25) that when Δvc_x diverges from zero, the direct modulation will inherently induce a fundamental frequency component within the circulating current. The inherently induced circulating current component due to the use of direct modulation has resulted in balance arm capacitor voltage, as shown in Fig. 11 (e) and Fig. 11(f). Thus, a balanced output voltage is achieved as illustrated in Fig. 11 (g)

In this case, the THD of phase-a voltage exhibited a slight increase from 17.40 % to 17.62 % after t = 0.5 s, while phase-b saw a minimal rise from 17.43 % to 17.44 %. Subsequently, after t = 1 s, the THD of phase-a decreased to 17.60 %, and phase-b also demonstrated a reduction to 17.38 %. These marginal variations in THD for both phases suggest that direct modulation is effective at preserving voltage quality during unbalanced power distribution.

In contrast, the indirect modulation method is not capable of inherently inducing a DC component and a fundamental frequency component within the circulating current, a limitation evident in Fig. 12 (a) Consequently, the arm capacitor voltage of phase-a and phase-b deviates from its ideal rating of 1500 V, as demonstrated in Fig. 12(b) and Fig. 12(c). This pronounced and fluctuating divergence in the arm capacitor voltage significantly disrupts the output voltage of phase-a and phase-b, leading to voltage imbalances as captured in Fig. 12(d).

The THD of phase-a voltage when the indirect modulation is used surged from 8.99 % to 23.90 % after $t_1 = 0.5$ s, and phase-b experienced a similar significant increase from 8.96 % to 23.10 %. Despite a subsequent slight decrease after $t_2 = 1$ s, to 22.80 % for phase-a and 23.98 % for phase-b, the THD levels remained substantially elevated compared to their initial values. This significant increase in THD underlines the challenges posed by indirect modulation in maintaining voltage quality under unbalanced power distribution conditions. It reinforces the potential need for additional controllers to introduce a DC component and a fundamental frequency component into the circulating currents to

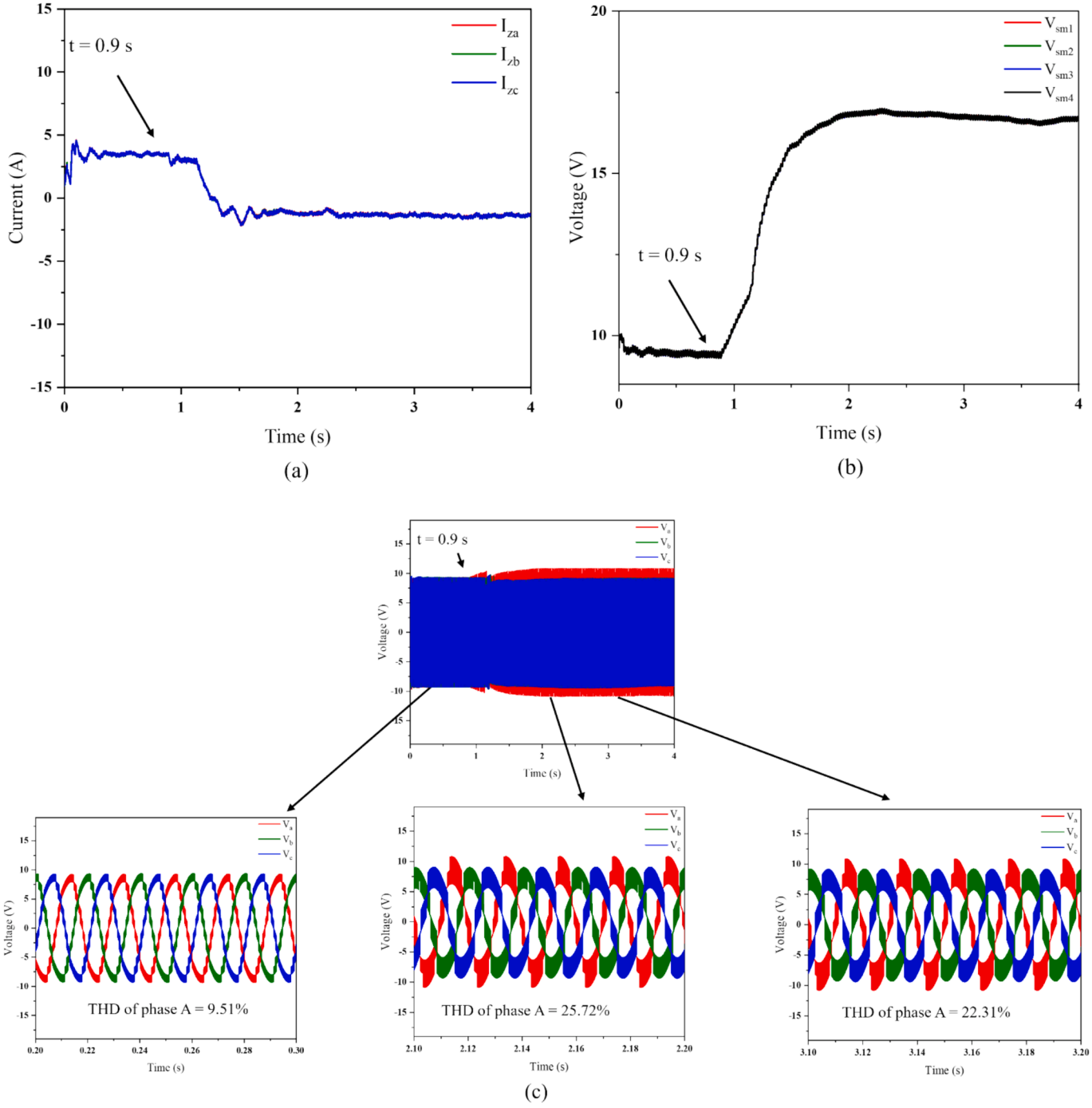

Fig. 8. Case 1: Indirect modulation a) Circulating current, b) SMs capacitor voltages, c) MMC output voltage.

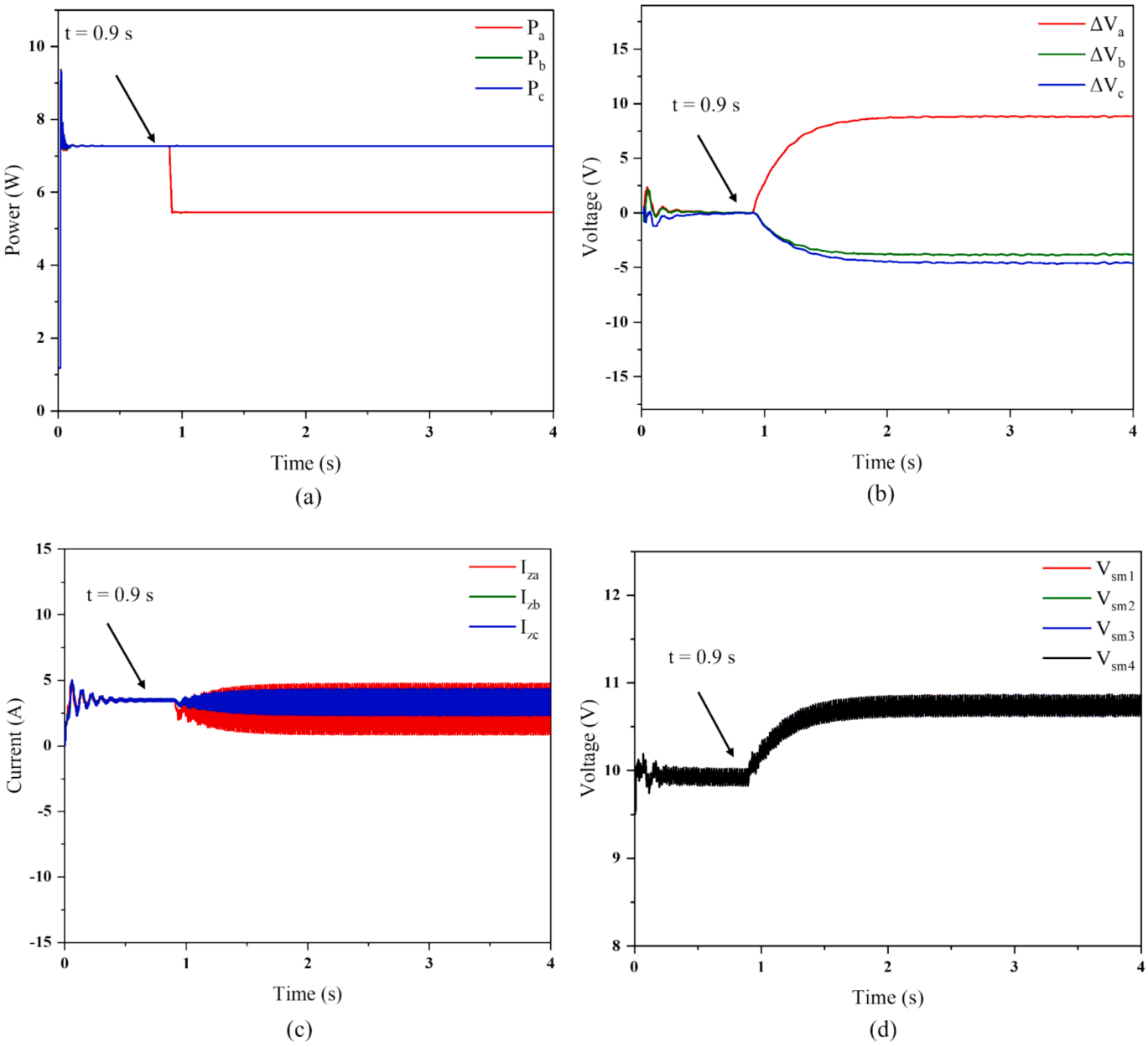

Fig. 9. Case 2: Direct modulation a) total power of microgrids, b) ΔV_x, c) Circulating current, d) SMs capacitor voltages, e) MMC output voltage.

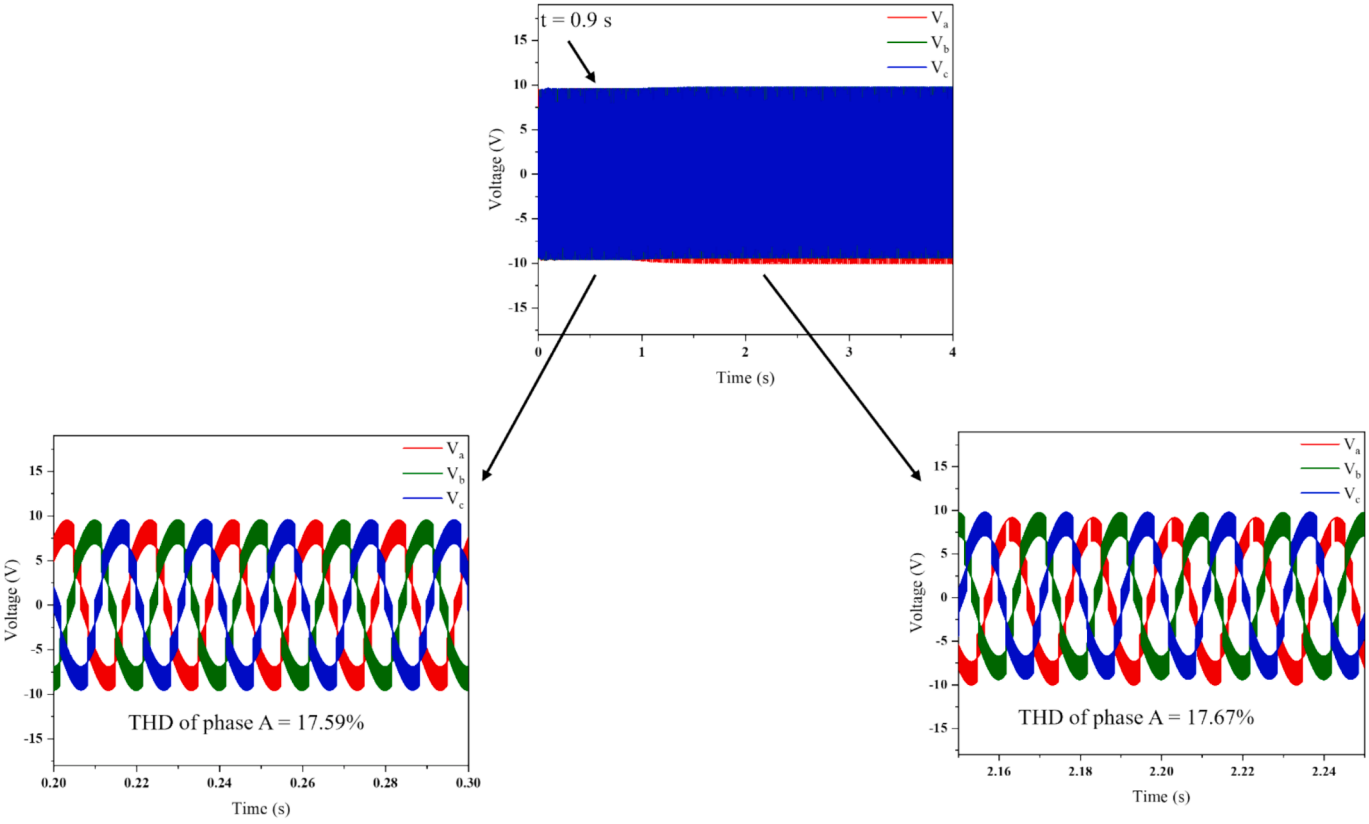

(e)

Fig. 9. (*continued*).

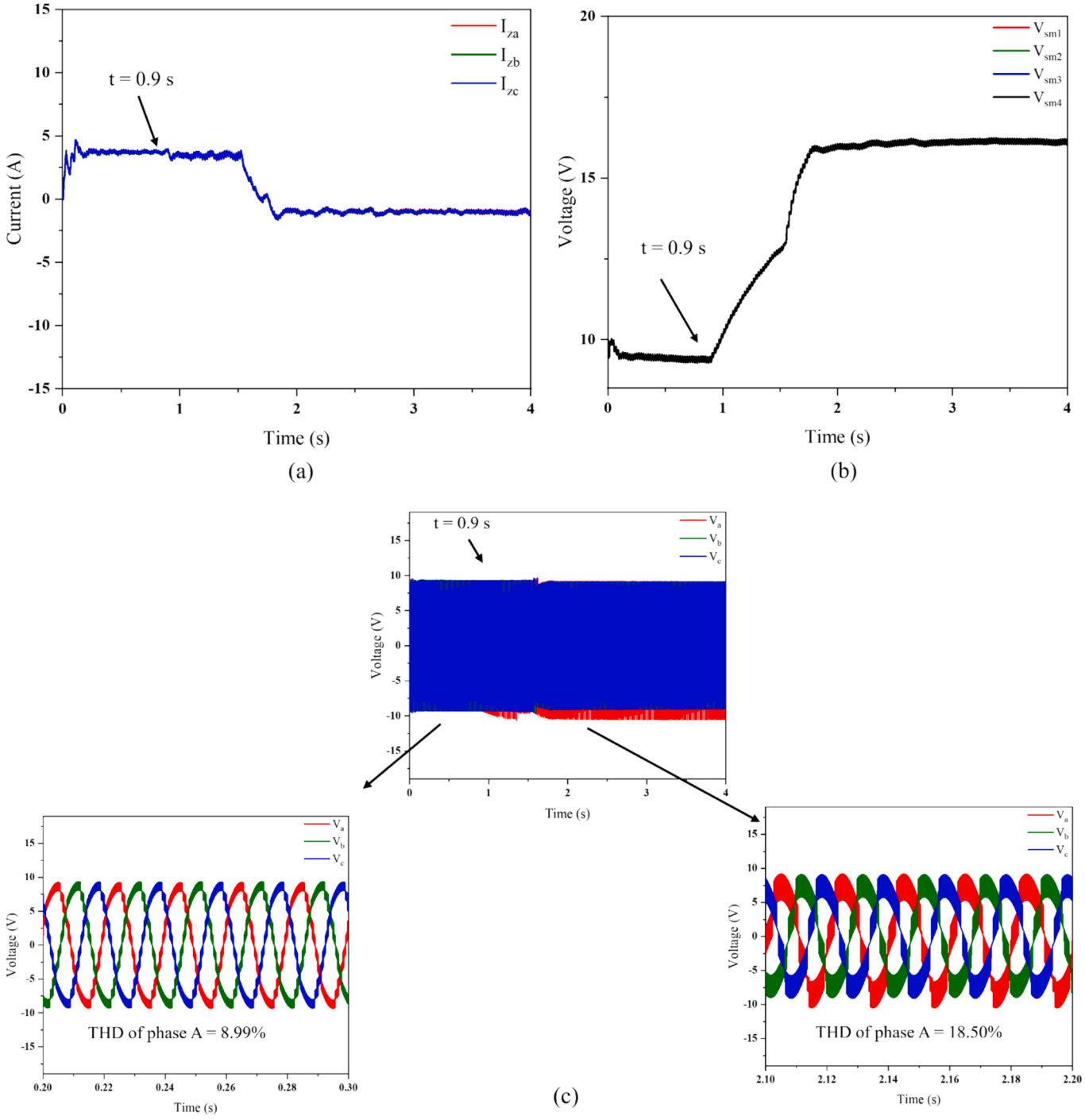

Fig. 10. Case 2: Indirect modulation a) Circulating current, b) SMs capacitor voltages, c) MMC output voltage.

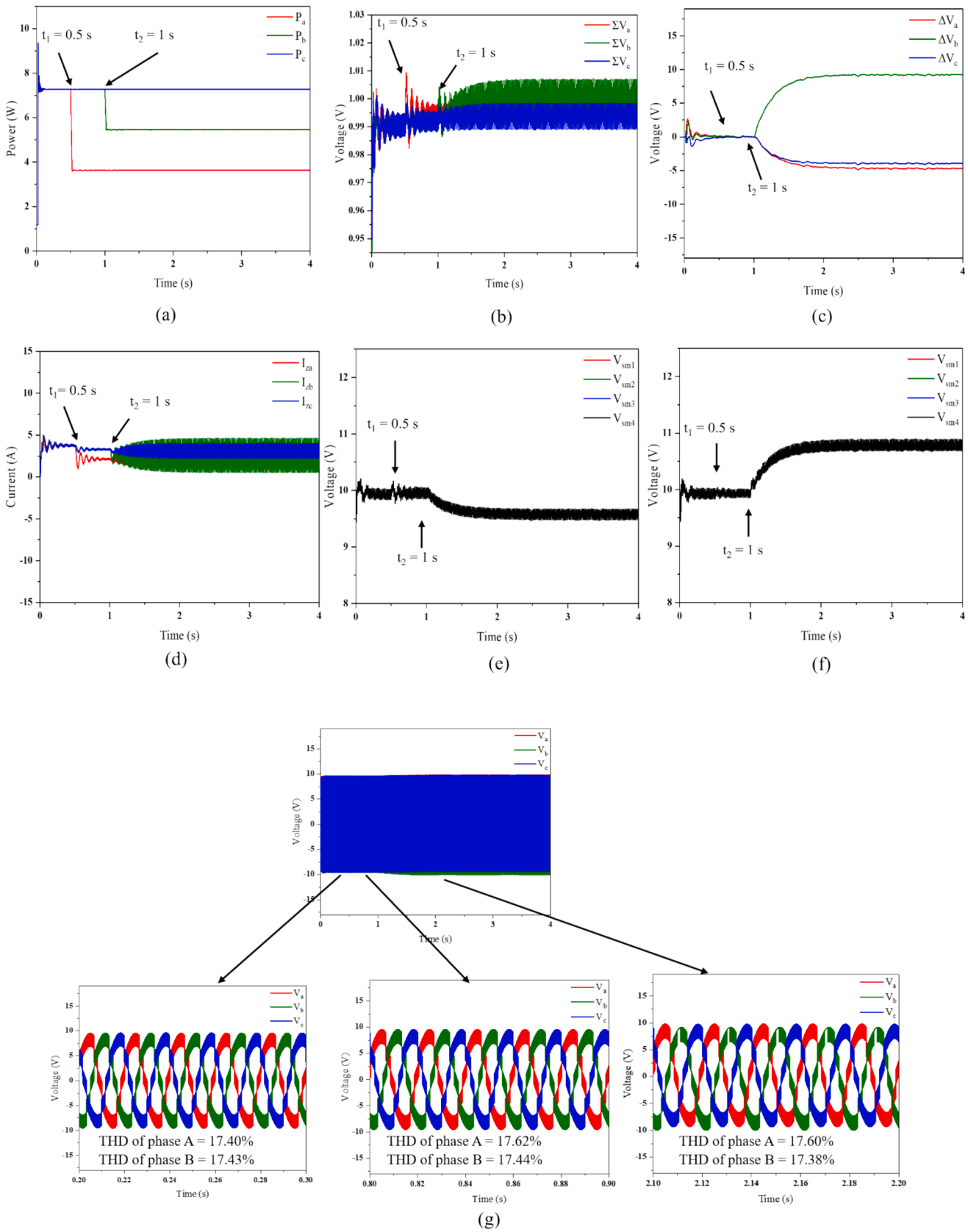

Fig. 11. Case 3: Direct modulation a) total power of microgrids, b) $\sum V_x$, c) ΔV_x, d) Circulating current, e) SMs capacitor voltages for phase-a, f) SMs capacitor voltages for phase-b, g) MMC output voltage.

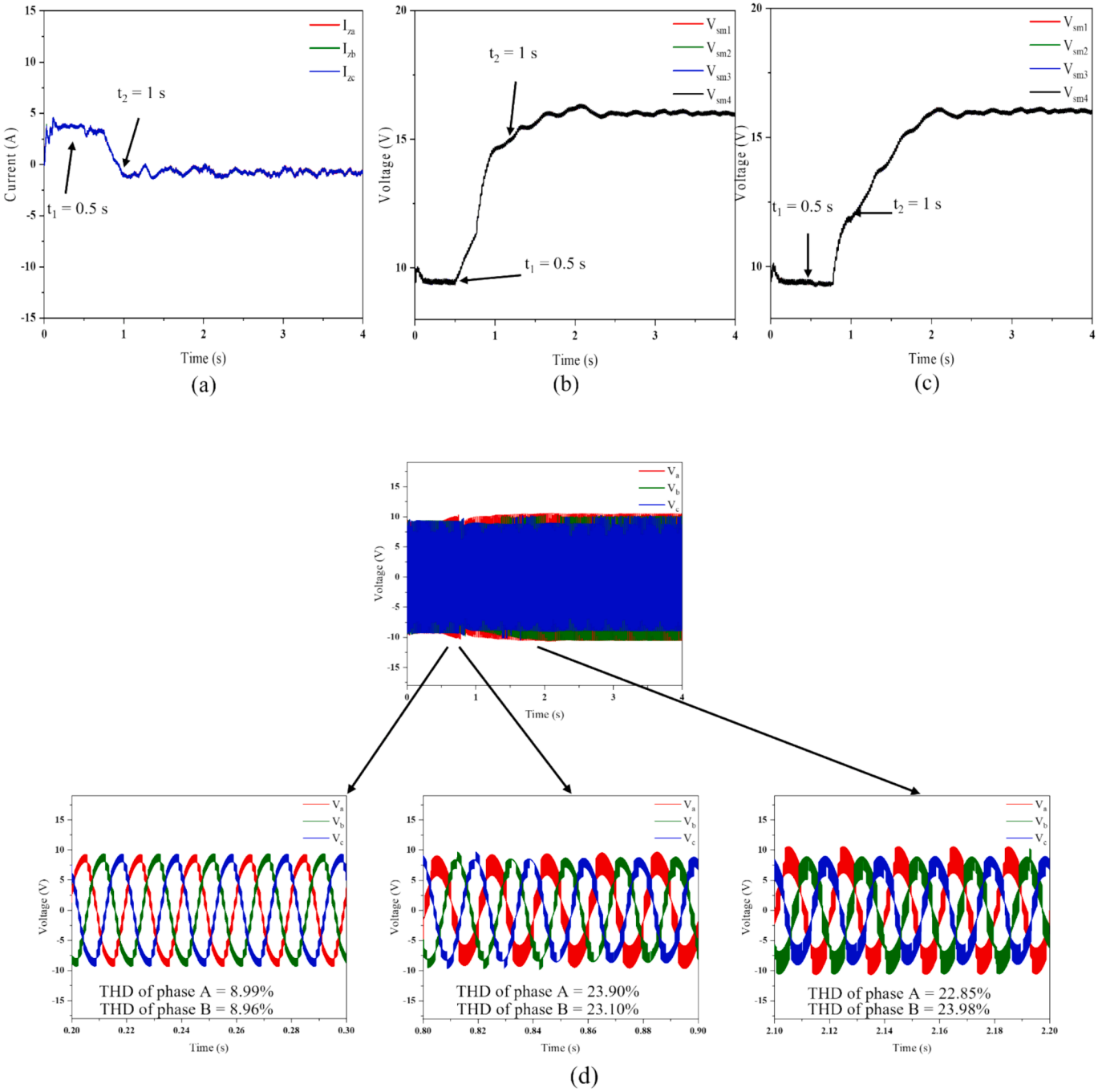

Fig. 12. Case 3: Indirect modulation a) Circulating current, b) SMs capacitor voltages of phase-a, c) SMs capacitor voltages of phase-b, d) MMC output voltage.

Table 4
Performance Comparison of Direct and Indirect Modulation Methods.

Method	Cases	**THD Variation** (Before and After events)	Circulating Current Component	Output Voltage Levels
Direct modulation	Case 1	Slight decrease from 17.56 % to 17.40 % of phase-a voltage	DC component	
	Case 2	Slight increase from 17.59 % to 17.67 % of phase-a voltage	AC and DC components	
	Case 3	- (Before and After t = 0.5 s phase-a voltage): Slight increase from 17.40 % to 17.62 %		
		- (Before and After t = 0.5 s −phase-b voltage): Slight increase from 17.43 % to 17.44 %	DC component	N + 1 levels
		- (Before and After t = 1 s phase-a): Slight decrease from 17.62 % to 17.60 %		
		- (Before and After t = 1 s phase-b): Slight decrease from 17.44 % to 17.38 %	AC and DC components	
Indirect modulation	Case 1	Significant increase from 9.51 % to 22.31 %	Non	
	Case 2	Significant increase from 8.99 % to 18.50 %	Non	
	Case 3	- (Before and After t = 0.5 s phase-a voltage): Significant increase from 8.99 % to 23.90 %	Non	2 N + 1 levels
		- (Before and After t = 0.5 s −phase-b voltage): Significant increase from 8.96 % to 23.10 %		
		- (Before and After t = 1 s phase-a): Slight decrease from 23.90 % to 22.80 %		
		- (Before and After t = 1 s phase-b): Slight increase from 23.10 % to 23.98 %	Non	

Table 5
Comparative assessment of key figure of merits between proposed direct modulation technique and Arm Energy and Circulating Current Controllers proposed in [22] and [24]

Figures of Merit	Proposed Direct Modulation Technique	Arm Energy and Circulating Current Controllers (Cascaded Control System) [22,24]
Key Control Components	Utilizes inherent generation of circulating current components (both fundamental and DC) within MMC without additional controllers.	Relies on multiple cascaded control loops with PI controllers, Proportional-Integral-Resonant (PIR) controllers.
System Complexity	Simplified control strategy with no need for additional controllers to balance arm capacitor voltages.	Higher complexity due to multiple control loops and requires precise delay, ensuring the inner loop operates faster than the outer loop to maintain system stability.
Tuning Requirements	No tuning required. Direct modulation inherently maintains voltage balance, reducing the need for extensive parameter adjustments.	Extensive tuning required, particularly for the PI and PIR controllers to ensure stable operation under varying conditions.
Performance under Unbalanced Conditions	Effectively balances arm capacitor voltages even under unbalanced power distribution, maintaining system stability.	Capable of balancing arm capacitor voltages, but performance heavily depends on accurate tuning, especially under unbalanced or fault conditions.
Robustness and Flexibility	High robustness and flexibility through the balancing of both arm and phases simultaneously.	In [22] the arm capacitor voltage balancing was only tackled, when unbalanced power distribution occurred between the arms. While, in [24] the unbalanced power distribution between the phases was investigated. The controller was not examined when arm and phase are both unbalanced in terms of power.
Computational Requirements	Lower computational requirements due to the simplicity of the control method, fewer calculations, and the use of only one CPS-PWM. The number of submodules (SMs) in the lower arm is determined by the complement of the upper arm, which removes the need for a second CPS-PWM. This reduces system computation burden and facilitates the inherent generation of DC and fundamental components in the circulating current during imbalanced power distribution.	Higher computational requirements due to the need to manage multiple control loops.

balance the arm capacitor voltage.

Table 4 provides a comparison of key performance indicators for direct and indirect modulation methods across the cases, further illustrating the effectiveness of the direct modulation approach.

Table 5 demonstrates the notable merits that the direct modulation technique holds in comparison with the proposed controllers in [22] and [24].

6. Conclusion

Balancing arm capacitor voltages is considered a critical challenge during unbalanced power distribution in MMC-based multiterminal hybrid microgrid systems. If left unresolved, this issue can significantly impact the balance of the output voltage of the MMC, thereby affecting the overall system performance. To address this challenge, this study proposes the use of direct modulation for the MMC-based multiterminal hybrid microgrid system, comprising of one MVAC microgrid and N LVDC microgrids that are interfaced with the MMC SMs.

The implementation of direct modulation provides a transformative solution that inherently generates both DC and fundamental frequency components within the MMC's circulating currents. These components play a pivotal role in stabilizing the arm capacitor voltages, thereby ensuring the production of a consistent output voltage at the MMC's output terminal.

The real-time simulation results confirm the superiority of direct modulation over the traditional indirect modulation approach. It was found that indirect modulation does not inherently induce DC and fundamental frequency components, necessitating the use of additional controllers to induce these components for arm capacitor voltage balancing. This requirement adds complexity to the system and can

compromise its efficiency. Consequently, direct modulation emerges as a more effective strategy for ensuring the seamless operation of an MMC-based multiterminal hybrid microgrid, particularly in scenarios characterized by imbalanced power distribution.

Notably, this study is the first to demonstrate the effectiveness of direct modulation in applications beyond HVDC, where power sources and loads are connected directly to the MMC's submodules. By showcasing that direct modulation can inherently address and rectify arm capacitor voltage imbalances without additional controllers, our work fills a significant gap in the literature, which provides a new perspective on optimizing MMC technology for complex microgrid structures.

Furthermore, future research will consider the implications of diverse types of loads and distributed generation resources to further examine the reliability of the direct modulation method and its effectiveness for the arm capacitor voltage balancing. This will provide effective solutions for successful usage of MMCs within multi-terminal hybrid microgrid.

CRediT authorship contribution statement

Ahmed G. Abo-Khalil: Writing – review & editing, Writing – original draft, Visualization, Validation, Supervision, Software, Resources, Project administration, Methodology, Investigation, Funding acquisition, Formal analysis, Data curation, Conceptualization. **Safia Babikir Bashir:** Writing – review & editing, Writing – original draft, Visualization, Validation, Software, Resources, Methodology, Investigation, Funding acquisition, Formal analysis, Data curation, Conceptualization. **Mena Maurice Farag:** Writing – review & editing, Writing – original draft, Validation, Investigation, Funding acquisition. **Ali A. Adam Ismail:** Writing – review & editing, Writing – original draft, Visualization, Validation, Supervision, Software, Resources, Project administration, Methodology, Investigation, Funding acquisition, Formal analysis, Data curation, Conceptualization. **Abdul-Kadir Hamid:** Writing – review & editing, Supervision, Project administration, Funding acquisition. **Nsilulu T Mbungu:** Writing – review & editing, Visualization, Validation, Supervision, Software, Resources, Project administration, Methodology, Investigation, Funding acquisition, Formal analysis, Data curation, Conceptualization. **Ramesh C. Bansal:** Writing – review & editing, Visualization, Supervision, Resources, Investigation, Funding acquisition, Formal analysis. **A. Elnady:** Writing – review & editing, Visualization, Validation, Supervision, Methodology, Investigation, Funding acquisition, Formal analysis. **Nirav Patel:** Writing – review & editing, Validation, Software, Resources, Methodology, Investigation.

Declaration of competing interest

The authors declare that they have no known competing financial interests or personal relationships that could have appeared to influence the work reported in this paper.

Data availability

Data will be made available on request.

References

[1] Najafzadeh M, Ahmadiahangar R, Husev O, Roasto I, Jalakas T, Blinov A. Recent Contributions, Future Prospects and Limitations of Interlinking Converter Control in Hybrid AC/DC Microgrids. IEEE Access 2021;9:7960–84. https://doi.org/10.1109/ACCESS.2020.3049023.

[2] Farag MM, Patel N, Hamid A-K, Adam AA, Bansal RC, Bettayeb M, et al. An Optimized Fractional Nonlinear Synergic Controller for Maximum Power Point Tracking of Photovoltaic Array Under Abrupt Irradiance Change. IEEE J Photovoltaics 2023;13:305–14. https://doi.org/10.1109/JPHOTOV.2023.3236808.

[3] Zheng J, Du J, Wang B, Klemeš JJ, Liao Q, Liang Y. A hybrid framework for forecasting power generation of multiple renewable energy sources. Renew Sustain Energy Rev 2023;172:113046. https://doi.org/10.1016/j.rser.2022.113046.

[4] Farag MM, Hamid A-K, AlMallahi MN, Elgendi M. Towards highly efficient solar photovoltaic thermal cooling by waste heat utilization: A review. Energy Convers Manag X 2024;23:100671. https://doi.org/10.1016/j.ecmx.2024.100671.

[5] Gutiérrez-Oliva D, Colmenar-Santos A, Rosales-Asensio E. A Review of the State of the Art of Industrial Microgrids Based on Renewable Energy. Electronics 2022;11:1002. https://doi.org/10.3390/electronics11071002.

[6] Farag MM, Bansal RC. Solar energy development in the GCC region – a review on recent progress and opportunities. Int J Model Simul 2022:1–21. https://doi.org/10.1080/02286203.2022.2105785.

[7] Arar Tahir K, Zamorano M, Ordóñez GJ. Scientific mapping of optimisation applied to microgrids integrated with renewable energy systems. Int J Electr Power Energy Syst 2023;145:108698. https://doi.org/10.1016/j.ijepes.2022.108698.

[8] Xiao Q, Chen L, Jia H, Wheeler PW, Dragicevic T. Model Predictive Control for Dual Active Bridge in Naval DC Microgrids Supplying Pulsed Power Loads Featuring Fast Transition and Online Transformer Current Minimization. IEEE Trans Ind Electron 2020;67:5197–203. https://doi.org/10.1109/TIE.2019.2934070.

[9] Uddin M, Mo H, Dong D, Elsawah S, Zhu J, Guerrero JM. Microgrids: A review, outstanding issues and future trends. Energy Strateg Rev 2023;49:101127. https://doi.org/10.1016/j.esr.2023.101127.

[10] Wei X, Xiangning X, Pengwei C. Overview of key microgrid technologies. Int Trans Electr Energy Syst 2018;28:e2566.

[11] Som S, De S, Chakrabarti S, Sahoo SR, Ghosh A. A Robust Controller for Battery Energy Storage System of an Islanded AC Microgrid. IEEE Trans Ind Informatics 2022;18:207–18. https://doi.org/10.1109/TII.2021.3057516.

[12] Sahoo S, Mishra S. A Distributed Finite-Time Secondary Average Voltage Regulation and Current Sharing Controller for DC Microgrids. IEEE Trans Smart Grid 2019;10:282–92. https://doi.org/10.1109/TSG.2017.2737938.

[13] Abhinav S, Modares H, Lewis FL, Davoudi A. Resilient Cooperative Control of DC Microgrids. IEEE Trans Smart Grid 2019;10:1083–5. https://doi.org/10.1109/TSG.2018.2872252.

[14] Chen S, Li P, Ji H, Yu H, Yan J, Wu J, et al. Operational flexibility of active distribution networks with the potential from data centers. Appl Energy 2021;293:116935. https://doi.org/10.1016/j.apenergy.2021.116935.

[15] Kang K-M, Choi B-Y, Lee H, An C-G, Kim T-G, Lee Y-S, et al. Energy Management Method of Hybrid AC/DC Microgrid Using Artificial Neural Network. Electronics 2021;10:1939. https://doi.org/10.3390/electronics10161939.

[16] Qiu H, Gu W, Pan J, Xu B, Xu Y, Fan M, et al. Multi-interval-uncertainty constrained robust dispatch for AC/DC hybrid microgrids with dynamic energy storage degradation. Appl Energy 2018;228:205–14. https://doi.org/10.1016/j.apenergy.2018.06.089.

[17] Wang C, Li X, Guo L, Li YW. A Nonlinear-Disturbance-Observer-Based DC-Bus Voltage Control for a Hybrid AC/DC Microgrid. IEEE Trans Power Electron 2014;29:6162–77. https://doi.org/10.1109/TPEL.2013.2297376.

[18] Mi Y, Zhang H, Fu Y, Wang C, Loh PC, Wang P. Intelligent Power Sharing of DC Isolated Microgrid Based on Fuzzy Sliding Mode Droop Control. IEEE Trans Smart Grid 2019;10:2396–406. https://doi.org/10.1109/TSG.2018.2797127.

[19] Nejabatkhah F, Li YW. Overview of Power Management Strategies of Hybrid AC/DC Microgrid. IEEE Trans Power Electron 2015;30:7072–89. https://doi.org/10.1109/TPEL.2014.2384999.

[20] Loh PC, Li D, Chai YK, Blaabjerg F. Autonomous Operation of Hybrid Microgrid With AC and DC Subgrids. IEEE Trans Power Electron 2013;28:2214–23. https://doi.org/10.1109/TPEL.2012.2214792.

[21] Wang R, Sun Q, Ma D, Liu Z. The Small-Signal Stability Analysis of the Droop-Controlled Converter in Electromagnetic Timescale. IEEE Trans Sustain Energy 2019;10:1459–69. https://doi.org/10.1109/TSTE.2019.2894633.

[22] Xiao Q, Mu Y, Jia H, Jin Y, Hou K, Yu X, et al. Modular multilevel converter based multi-terminal hybrid AC/DC microgrid with improved energy control method. Appl Energy 2021;282:116154. https://doi.org/10.1016/j.apenergy.2020.116154.

[23] Briz F, Lopez M, Rodriguez A, Arias M. Modular Power Electronic Transformers: Modular Multilevel Converter Versus Cascaded H-Bridge Solutions. IEEE Ind Electron Mag 2016;10:6–19. https://doi.org/10.1109/MIE.2016.2611648.

[24] Xiao Q, Mu Y, Jia H, Jin Y, Yu X, Teodorescu R, et al. Novel modular multilevel converter-based five-terminal MV/LV hybrid AC/DC microgrids with improved operation capability under unbalanced power distribution. Appl Energy 2022;306:118140. https://doi.org/10.1016/j.apenergy.2021.118140.

[25] Lachichi A, Junyent-Ferre A, Green TC. Comparative Optimization Design of a Modular Multilevel Converter Tapping Cells and a 2L-VSC for Hybrid LV ac/dc Microgrids. IEEE Trans Ind Appl 2019;55:3228–40. https://doi.org/10.1109/TIA.2019.2897263.

[26] Bashir SB, Ismail AAA, Elnady A, Farag MM, Hamid A-K, Bansal RC, et al. Modular Multilevel Converter-Based Microgrid: A Critical Review. IEEE Access 2023;11:65569–89. https://doi.org/10.1109/ACCESS.2023.3289829.

[27] Motwani JK, Liu J, Boroyevich D, Burgos R, Zhou Z, Dong D. Modeling and Control of a Hybrid Modular Multilevel Converter for High-AC/Low-DC Medium-Voltage Applications. IEEE Trans Power Electron 2024;39:5371–85. https://doi.org/10.1109/TPEL.2024.3361908.
[28] Yin J, Dai N, Leon JI, Perez MA, Vazquez S, Franquelo LG. Common-Mode-Voltage Regulation of Modular Multilevel Converters Through Model Predictive Control. IEEE Trans Power Electron 2024:1–14. https://doi.org/10.1109/TPEL.2024.3377203.
[29] Zadeh AH, Ahmadi S, Neyshabouri Y, Asadi E, Iman-Eini H, Liserre M. An Enhanced Model Predictive Capacitor Voltage Control of Hybrid Modular Multilevel Converters Under Over-Modulation Circumstances. IEEE Trans Power Electron 2024:1–13. https://doi.org/10.1109/TPEL.2024.3365850.
[30] Li Z, Pei Y, Chen L, Wang L, Wang J. A Novel Inductance and Capacitance Selection Method for Modular Multilevel Converters Based on Modulation Margin Considerations. IEEE J Emerg Sel Top Power Electron 2024:1. https://doi.org/10.1109/JESTPE.2024.3379206.
[31] Allebrod S, Hamerski R, Marquardt R, New transformerless, scalable Modular Multilevel Converters for HVDC-transmission. IEEE Power Electron. Spec. Conf. IEEE 2008;2008:174–9. https://doi.org/10.1109/PESC.2008.4591920.
[32] Gnanasambandam K, Rathore AK, Edpuganti A, Srinivasan D, Rodriguez J. Current-Fed Multilevel Converters: An Overview of Circuit Topologies, Modulation Techniques, and Applications. IEEE Trans Power Electron 2017;32:3382–401. https://doi.org/10.1109/TPEL.2016.2585576.
[33] Bashir SB, Beig AR. An improved voltage balancing algorithm for grid connected MMC for medium voltage energy conversion. Int J Electr Power Energy Syst 2018;95:550–60. https://doi.org/10.1016/j.ijepes.2017.09.002.
[34] Solas E, Abad G, Barrena JA, Carear A, Aurtenetxea S. Modelling, simulation and control of Modular Multilevel Converter. Proc. 14th Int. Power Electron. Motion Control Conf. EPE-PEMC 2010, IEEE; 2010, p. T2-90-T2-96. Doi: 10.1109/EPEPEMC.2010.5606881.
[35] Zhang L, Tang Y, Yang S, Gao F. Decoupled Power Control for a Modular-Multilevel-Converter-Based Hybrid AC–DC Grid Integrated With Hybrid Energy Storage. IEEE Trans Ind Electron 2019;66:2926–34. https://doi.org/10.1109/TIE.2018.2842795.
[36] Debnath S, Qin J, Bahrani B, Saeedifard M, Barbosa P. Operation, Control, and Applications of the Modular Multilevel Converter: A Review. IEEE Trans Power Electron 2015;30:37–53. https://doi.org/10.1109/TPEL.2014.2309937.
[37] Antonopoulos A, Ängquist L, Nee HP. On dynamics and voltage control of the modular multilevel converter. 2009 13th Eur Conf Power Electron Appl EPE '09 2009:1–10.
[38] Dekka A, Wu B, Zargari NR, Fuentes RL. A Space-Vector PWM-Based Voltage-Balancing Approach With Reduced Current Sensors for Modular Multilevel Converter. IEEE Trans Ind Electron 2016;63:2734–45. https://doi.org/10.1109/TIE.2016.2514346.
[39] Dekka A, Wu B, Zargari NR, Fuentes RL. Dynamic Voltage Balancing Algorithm for Modular Multilevel Converter: A Unique Solution. IEEE Trans Power Electron 2016;31:952–63. https://doi.org/10.1109/TPEL.2015.2419881.